Journal of Magnetism and Magnetic Materials 519 (2021) 167469

Contents lists available at ScienceDirect

Journal of Magnetism and Magnetic Materials

journal homepage: www.elsevier.com/locate/jmmm

Research articles

High-frequency power loss mechanisms in ultra-thin amorphous ribbons

Ansar Masood[a,*], H.A. Baghbaderani[a], K.L. Alvarez[b], J.M. Blanco[c], Z. Pavlovic[a], V. Ström[d], P. Stamenov[e], C.O. Mathuna[a], P. McCloskey[a]

[a] Micro & Nano Systems Centre, Tyndall National Institute, University College Cork (UCC), Lee Maltings, Dyke Parade, T12 R5CP Cork, Ireland
[b] CEIT-Basque Research and Technology Alliance (BRTA), Manuel Lardizabal 15, 20018 Donostia / San Sebastián, Spain
[c] Department of Applied Physics I, Faculty of Engineering Gipuzkoa, University of the Basque Country, San Sebastián, Spain
[d] Materials Science and Engineering Department, KTH-Royal Institute of Technology, Brinellvägen 23, S100 44, Stockholm, Sweden
[e] School of Physics and CRANN, Trinity College Dublin, 43 Pears street, Dublin 2, Ireland

ARTICLE INFO

Keywords:
Soft magnetic materials
Amorphous alloys
Ultra-thin ribbons
High-frequency applications
Materials loss mechanisms
Eddy current loss
Excess loss

ABSTRACT

Soft magnetic amorphous materials with ultra-low power loss are highly desirable for high-frequency drive applications. The present work demonstrates the high-frequency power loss performance and underlying loss mechanisms in ultra-thin amorphous alloys. This is achieved by rapid-quenching amorphous alloys of Co-, CoFe- and Fe-rich systems, investigating their amorphous atomic structure, quantifying the saturation magnetostriction constants (λ_s), imaging magnetic domains at remanent magnetization, analyzing magnetization reversal from various magnetization levels, and finally, investigating the material loss performance over a broad frequency range (f = 50 kHz–2 MHz) at various excitation levels (B_m = 25–100 mT). The ultra-high performance of ultra-thin Co-rich amorphous ribbons, as compared to CoFe- and Fe-rich alloys, was attributed to the significantly low eddy current loss, due to the reduced thickness, and a minimal amount of excess loss, owning to minimal magnetoelastic contributions and magnetization reversal by rotation. The underlying loss mechanisms were analyzed by decomposing material loss into primary components and identifying the magnetization reversal mechanisms using minor hysteresis loops. In the Co-rich amorphous alloys, we suggest that magnetization reversal by rotation dominates, at least at low excitations, while in CoFe- and Fe-rich alloys domain wall displacement prevails and contributes significantly to the excess loss up to the MHz frequency range. Magnetization reversal by rotation in Co-rich alloys could be attributed to the zero/near-zero λ_s, and eventually low residual stress, leading to a homogeneous magnetic domain structure, as compared to the inhomogeneous "fingerprint-like" complex domains in highly magnetostrictive CoFe-rich alloys.

1. Introduction

Recent advances in power conversion circuits have pushed their switching frequencies to 100s of kHz and even into the megahertz range [1–3]. The size of passive components, which occupy almost 30% volume fraction, is the main challenge in the miniaturization of power converters [4]. As a case in point, despite having ultra-low loss performance, the low magnetic flux density ($\leq$0.5 T) of ferrites is a critical roadblock in miniaturizing the passive component technology [5]. Thus, the development of high-flux density low-loss soft magnetic materials to replace the best-in-class bulky ferrite passive components is a significant challenge to attain the miniaturized power converters at high frequencies [6].

The high-flux density (B_s > 1.8 T), high-permeability ($\mu > 10^5$), ultra-low coercivity (H_c < 10 A/m), and high electrical resistivity (> 100 μΩ cm) of amorphous metals make them a potential soft magnetic material for device miniaturization in high-frequency applications [6–9]. The single largest example of commercially available amorphous alloys is melt-spun ribbons that have a thickness in the range of 20–30 μm and are widely used in low-frequency (50–60 Hz) power distribution transformers [6]. However, as the operating frequency (f) of device approaches kHz range, the eddy-current loss ($P_{eddy} \propto f^2$) sharply increases as compared to the hysteresis loss ($P_{hys} \propto f$) and eventually, the total core loss is dominated by P_{eddy} at f > 100 kHz [4,7]. At high frequencies, the eddy current loss generates a tremendous amount of Joule heat and, consequently, complicates the design engineering of the energy storage/conversion devices. Eddy current losses can be dramatically reduced by eliminating the electrically conducting path using high resistivity magnetic materials. The electrical resistivity of amorphous alloys is significantly higher (~3×) than their crystalline

* Corresponding author.
E-mail address: ansar.masood@tyndall.ie (A. Masood).

https://doi.org/10.1016/j.jmmm.2020.167469
Received 10 March 2020; Received in revised form 23 July 2020; Accepted 1 October 2020
Available online 15 October 2020

counterparts, however, at the same time, it is substantially lower than the best-in-class ferrites. To demonstrate an advantage of high-flux density amorphous alloys at high frequencies, the authors have investigated two different approaches to produce ultra-thin soft magnetic ribbons [6,10]. The in-situ thinning of melt-spun amorphous ribbons revealed significant economic advantages, over the post-processing route of chemical etching, for high-frequency power applications. However, the fundamental mechanisms responsible for material loss at high frequencies in ultra-thin ribbons produced by in-situ rapid quenching yet need to be explored [6].

Fundamental mechanisms responsible for material losses at high frequencies depend on the type of domain walls and the nature of the magnetization reversal through domain wall displacement or magnetization rotation. In the present work, we demonstrate the high-frequency material performance and underlying loss mechanisms in rapidly quenched ultra-thin amorphous ribbons of Co-, CoFe-, and Fe-rich alloys. The advantage of zero/near-zero magnetostrictive ultra-thin Co-rich amorphous alloys for high-frequency applications, over Fe-rich amorphous alloys, has been demonstrated and discussed in relation to low magnetostriction constants, λ_s, the nature of magnetic domains, and their magnetization reversal through the magnetization rotation using minor hysteresis loops.

2. Experimental methods

Arc-melting using high-purity (at least 99.99%) elements in an argon-flow atmosphere was used to produce 20–30 g ingots of $Co_{67}Fe_4Mo_2Si_{16}B_{11}$ (Co-rich), $Co_{47.6}Fe_{20.4}Nb_5Si_{5.1}B_{21.9}$ (CoFe-rich), and $Fe_{71}Ni_{14}B_{23}Nb_4$ (Fe-rich) alloys. Alloy compositions are presented in atomic %. From now on, for simplicity, the name of alloys is used as Co-rich, CoFe-rich, and Fe-rich alloys. In order to avoid oxidation of ingots, one arc was fixed to melt the titanium ingot, which was used as a getter material. The ingots were melted at least ten times (5-times each side) to achieve a homogeneous composition of the alloys. In the second step, the ingots were crushed into small pieces and remelted by induction before the rapid quenching process. A single roller melt spinner was used to quench the amorphous ribbons of different thicknesses (5–18 μm), which were produced by varying the speed of the copper wheel in an inert atmosphere. The detailed procedure for the production process of ultra-thin ribbons is reported elsewhere [6]. The ultra-thin (~5 μm) and 18 μm ribbons were only used for the high-frequency performance comparison.

The structural analysis of the samples was carried out using X-ray diffraction (XRD) technique using Cu-$K\alpha$ radiation of $\lambda = 1.54$ Å (Siemens 5000). Thermal properties of the amorphous ribbons were characterized using differential scanning calorimetry (TA Instruments, DSC 2920) at the heating rate of 10 K /min. The temperature dependence of magnetization, *M(T),* of ribbons was performed using a magneto-thermo-gravimetry (MTG). The Curie temperature (T_c) of the alloys was measured at the steepest temperature derivative, d*M(T)/dT,* of the *M(T)* curve, the detailed procedure is published elsewhere [11].

Saturation magnetostriction (λ_s) was measured using a small-angle magnetization rotation (SAMR) process; the detailed procedure is published elsewhere [12]. Magnetic domains were imaged using a magneto-optical Kerr effect microscope (Evico Magnetics Kerr Microscope & Magnetometer) after polishing the ribbon samples to a high level of smoothness. The magnetization reversal of the ribbons was studied using a BH-loop tracer (SHB Mesa-200) at the sample length of 2.5 cm at room temperature.

The power loss characterization of the ribbons was performed using a custom design air-core solenoid inductor. The inductor was constructed from 150 turns of 28 gauge Cu wire wound onto a 5 cm long hollow cylinder of 5 mm outer radius with near-zero spacing between the turns to create a uniform excitation field inside the solenoid. The impedance of the air core solenoid, Z_a, was measured using an LCR meter (HP4284A) at various excitation current levels. The ribbon samples of 20 mm length were fixed on a sample holder and inserted inside the solenoid, along its axis, where the uniformity of the field is best. Without moving the probes from the test fixture, the ribbons were centered inside the solenoid, to be at the same distance from both open ends, where the field lines are no longer parallel to the axis. In this way, the magnetic core material was exposed to a uniform excitation field along its length. The Cu turns are at a sufficient distance from the solenoid axis so that the demagnetization field does not alter the field lines around the turns, maintaining the same AC winding resistance as in the case of air-core solenoid measurement. Therefore, the difference between the impedance measurement with and without magnetic core material, Z_c, and Z_a, respectively represents the contribution of the magnetic core to the inductance and power loss at each particular frequency. As the cross-sectional area of the ribbons is significantly smaller than that of the solenoid, the effect of the insertion of the magnetic core on the real part of the inductance is negligible. Thus, the magnetic material power loss is calculated as;

$$P_{lass} = R_e(Z_c - Z_a)I^2 \tag{1}$$

where Re(Z_c-Z_a) is the real part of the complex impedance difference, and I is the excitation current measured using the LCR meter. The induction field inside the ribbon samples is calculated by;

$$B = \frac{lm(Z_c - Z_a)I}{(2\pi fS)}\pi r^2 \tag{2}$$

where f and S are the measurement frequency and the total cross-sectional area of the ribbons, and r is the radius of the coils. The power loss measurement method was tested with commercial amorphous and nanocrystalline alloys, and the results were in good agreement with the reported power loss in the standard datasheets.

3. Results and discussion

The microscopic structural analysis of the Co-, CoFe- and Fe-rich alloys was investigated using X-ray diffraction analysis (not shown here). A broad-maxima in the range of $2\theta = 40$–50° and the absence of Bragg's peak in XRD pattern of both ultra-thin and 20 μm ribbons confirmed the disorder amorphous atomic structure of the as-quenched alloys. The atomic structure of the amorphous ribbons was further investigated measuring the *M(T)* of the melt-spun alloys, as presented in Fig. 1. All ribbons revealed a single-phase *M (T)* behavior, instead of showing any multi-phase "kink", until reaching the Curie point. The single-phase *M(T)* response confirmed that investigated alloys were monolithic amorphous, and retained the crystallization temperature above T_c of the amorphous phase. The *M(T)* of Co-rich ultra-thin ribbons is also shown for comparison. The overlapped *M (T)* curves of ultra-thin ~5 μm and ~18 μm ribbons confirmed the uniform

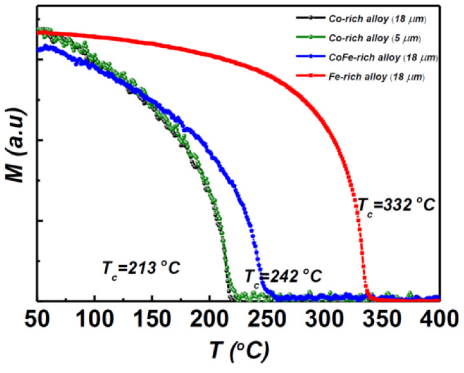

Fig. 1. The monotonic temperature dependence of magnetization, *M (T)*, shows the amorphous nature of the melt-spun Co-rich alloys ($T_c = 213$ °C), (b) CoFe-rich alloys ($T_c = 242$ °C), (c) Fe-rich alloys ($T_c = 332$ °C). The T_c of alloys was measured at the steepest temperature derivative, *dM/dT*, of the *M(T)*.

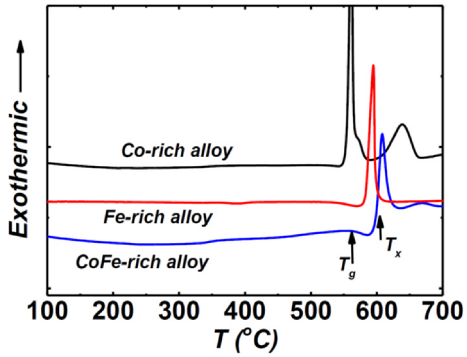

Fig. 2. The differential scanning calorimetry (DSC) trace of as-quenched ribbons of Co–, CoFe-, and Fe-rich alloys. The glass transition temperature (T_g), crystallization temperature (T_x), and supercooled region ($\Delta T_x = T_x$-T_g) are marked on the traces.

homogenous amorphous atomic structure of ribbons produced under different experimental conditions (i.e., speed of Cu-wheel = 3500–5100 rpm) [6]. The Curie point, shape and area under the *M(T)*curve depend on nature and quantity (vol. %) of the phase and have been found to be useful to trace small structural changes in amorphous materials [6,13].

Fig. 2 presents the DSC traces of the Co-, CoFe-, and Fe-rich amorphous alloys. The glass transition temperature (T_g), crystallization temperature (T_x), supercooled region ($\Delta T_x = T_x$-T_g), peak temperatures (T_p) and crystallization enthalpy (ΔH_C) were measured using DSC traces, and summarized in Table 1. The CoFe-rich alloy revealed the highest T_g, T_x, and T_p as compared to Co-rich alloy. However, the ΔT_x of Co-rich alloy was found to be broader than the other investigated alloys. The different nature of crystallization behaviors as a function of temperature is evident from the DSC patterns (Fig. 2). The CoFe-rich alloy showed a two-stage crystallization behavior before complete melting. The two-stage crystallization behavior started to vanish by showing a small exothermic peak, along with a narrow temperature range between the exothermic events, when Co-rich alloys were substituted with a high concentration of Fe (~20 at. %). Finally, the crystallization mechanism transformed into a single stage for Fe-rich glassy alloys, which suggests a eutectic crystallization is taking place [14].

The presence of ΔT_x in the DSC patterns of all investigated alloys reveals the glassy nature and hence confirms the highly stable amorphous atomic structure as compared to conventional amorphous alloys. The large ΔT_x (=47.11 K) of Co-rich ribbons, as compared to CoFe- and Fe-rich alloys, shows higher glass forming ability (GFA), which is considered another instrument to measure the soft magnetic properties of amorphous materials [7]. The glassy alloys with large ΔT_x are expected to show enhanced soft magnetic properties as compared to conventional amorphous alloys [15]. The enhanced soft magnetic properties are due to the small number of quasidislocation dipole (QDDs)-type defects in glassy alloys, as compared to conventional amorphous alloys, which were originally considered sources of elastic stress or pinning sites for the domain walls during displacement [15]. Piccino *et al.* [16] investigated the frequency dependence of materials loss performance of the glassy alloys with different GFA and revealed the better performance of high GFA alloys. To conclude, the structural, thermal, and magneto-thermal analysis of ribbons confirms the highly stable disordered atomic structure of the investigated alloys in the as-quenched state.

Fig. 3 presents the power loss density (P) of Co-, CoFe-, and Fe-rich melt-spun glassy alloys over a broad frequency spectrum (f = 50 kHz–2 MHz) and excitation fields (B_m = 25–100 mT). The power loss density of Co-rich alloys was significantly improved by reducing the ribbon thickness from 18 to 5 μm. For Co-rich melt-spun alloys, for example, the P reduced from 2591 to 253 W/kg at f = 300 kHz (B_m = 100 mT), revealing ~10× improvement in material loss performance. Similarly, the P reduced from 253 to 42 W/kg at f = 2 MHz (B_m = 10 mT) by reducing the ribbon thickness, which represents a ~6× improvement in materials loss performance. However, the improvement in P after thinning the amorphous ribbons for CoFe- and Fe-rich alloys was not significant. For example, for CoFe-rich amorphous alloys, the power loss density reduced from 2271 to 1245 W/kg on thickness reduction from 18 μm to 5 μm at f = 300 kHz (B_m = 100 mT), which is only ~1.8× improvement in the material loss performance. Similarly, the P of the amorphous ribbons was reduced from 236 to 98 W/kg at f = 2 MHz (B_m = 10 mT) on thickness reduction by revealing ~2× improvement. Similar trends in the improvement of P of Fe-rich amorphous alloys were observed, showing the ~1.5× improvement at f = 300 kHz (100 mT) and ~1.6× improvement at 2 MHz (10 mT) after thinning the ribbons.

A marginal improvement in the power loss density of CoFe- and Fe-rich amorphous alloys, as compared to Co-rich alloy, by thinning the ribbons to 5 μm is surprising, and points outs an interesting question to further explore in relation to the fundamental loss mechanisms in soft magnetic amorphous alloys of different systems.

According to the statistical theory of material loss separation, the total power loss (P) of magnetic materials can be broadly divided into three different mechanisms, such as hysteresis loss (P_{hys}), eddy current loss (P_{eddy}), and excess loss (P_{exc}) [10,17]. The P of the materials can be expressed as:

$$P = P_{hys} + P_{eddy} + P_{exc} \tag{3}$$

The area of the hysteresis loop that originates due to short-range magnetization reversal mechanisms, such as magnetic moment reversal modes, pinning of magnetic domain walls, effective magnetic anisotropies, and size distribution of grains, governs the P_{hys} of the materials [16,17]. The P_{hys} becomes independent of frequency due to the short response time of the mechanisms discussed earlier [17]. On the other hand, P_{eddy} is a dynamic macroscopic loss and is independent of the magnetic domain structure [17]. Contrary to P_{eddy}, P_{exc} strongly relates to the intermediate length scales of magnetic domains [16,17]. Considering the sinusoidal waveform and rectangular dimensions of ribbons, P_{eddy} can be described by the following equation [16].

$$P_{eddy} = (\pi^2/6)\sigma t^2 B_m^2 f^2 \tag{4}$$

where t is the thickness of the ribbons, and σ is the conductivity of the material. Under the same assumptions as mentioned above, the analytical expression for the P_{exc} can be expressed as [18–20]:

$$P_{exc} = 8.76(\sigma G A \delta)^{1/2} B_m^{3/2} f^{3/2} \tag{5}$$

where G = 0.1356 is a dimensionless coefficient, A is the cross-

Table 1
The glass transition temperature (T_g), crystallization temperature (T_x), supercooled region ($\Delta T_x = T_x$-T_g), peak temperature (T_p), and crystallization enthalpy (ΔH_C) of Co–, CoFe-, and Fe-rich alloys measured using the differential scanning calorimetry (DSC).

Sample	T_g (°C)	T_x (°C)	ΔT_x (T_x-T_g)	T_p (°C)	H (J/g)
Co-Fe-Mo-B-Si (Co-rich alloy)	508.71	555.82	47.11	561.69	144.00
Co-Fe-Nb-B-Si (CoFe-rich alloy)	563.40	597.33	33.92	603.01	67.77
Fe-Ni-B-Nb (Fe-rich alloy)	538.01	581.02	43.01	594.8	6.44

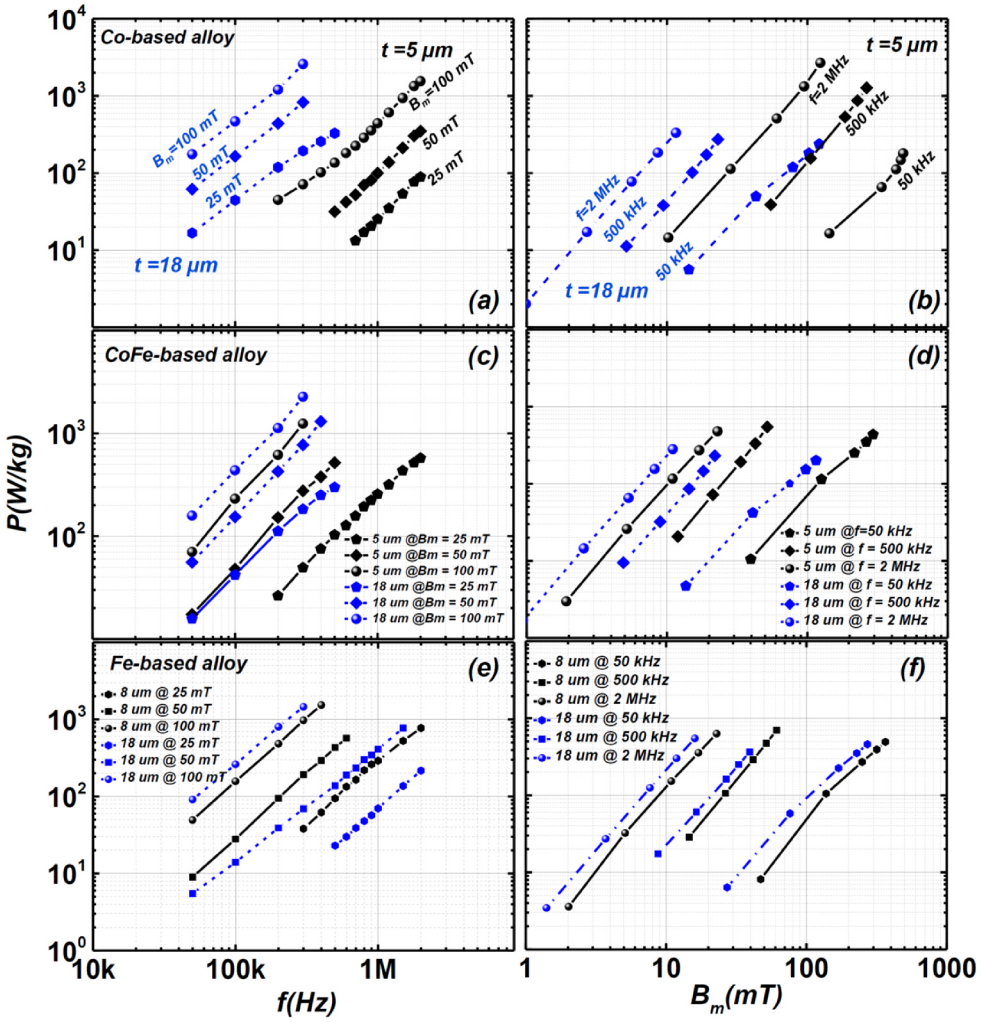

Fig. 3. (a) Power loss density (P) of in-situ thinned amorphous ribbons over a broad frequency (f) spectrum and excitation fields (B_m). (a), (b) Co-rich alloy, (c), (d) CoFe-rich alloy, (e), (f) Fe-rich alloy.

sectional area, and δ is a field constant which directly depends on domain wall pinning. For magnetic cores, the P is frequency-dependent and largely depends on the hysteresis and eddy current losses at low frequencies (≤100 kHz). However, the excess loss, which is due to localized eddy currents around the moving domain walls, dominates at > kHz frequency range in amorphous materials [21]. Core loss per cycle (P/f) of ultra-thin ribbons was analyzed (see Fig. 4) to understand the material's loss mechanism over a broad frequency range. The behavior of P/f verses f should be linear if eddy current loss is dominant, and the slope of the curve should give its magnitude [22]. The nonlinear behavior of P/f of the ultra-thin alloys (see Fig. 4) shows a change in the material loss mechanism at higher frequencies. The inflection point in the P/f verses f is strictly dependent on the B_m of the alloys. Interestingly, the infection point for Co-rich alloys appeared at significantly higher frequencies as compared to CoFe- and Fe-rich alloys at all excitation fields (B_m = 10–100 mT). For example, Co-rich alloy showed the transition at 1 MHz (B_m = 50 mT), while CoFe- and Fe-rich alloys revealed the same transition in the range of 200 kHz. Furthermore, the slope of the first linear section of the P/f verses f curve of Co-rich alloy is significantly lower, as compared to other investigated alloys, which confirm the existence of small eddy current loss in the material. The change in the slope of P/f (shown as the dashed line in Fig. 4) indicates a significant contribution of excess loss in the investigated alloys when frequency approaches the high kHz to MHz range for different alloy systems. Alvarez *et al.* [13] and Suzuki *et al.* [23], separately, observed a similar transition in the material loss of amorphous cores and correlated it to the domination of excess loss at particular frequencies. We believe the sharp transition in P/f of the ultra-thin ribbons at high frequencies is due to the remarkable increase in the excess loss of the alloys. The transition behavior of Co-rich alloys at higher frequencies, as compared to CoFe- and Fe-rich alloys, make them a material of choice for high-frequency drive applications.

Detailed information on the frequency dependence of materials loss performance and microstructural parameters can be extracted using the theory of magnetic loss separation without a precise description of the magnetization reversal process for a broadband frequency spectrum [16,17,19]. The material's loss of Co-rich and CoFe-rich alloys (5 and 18 μm) was decomposed into the primary loss components (see Fig. 5). The eddy current and excess loss in Co-rich alloys reduced significantly on thickness reduction, while a minimal reduction in the excess loss was observed in the CoFe-rich alloys. A sharp transition in the excess loss of Co-based alloys was observed at 1 MHz, while a similar transition was observed in CoFe-rich alloys at much lower frequencies. Interestingly, the slope after the inflection point for CoFe-rich alloys is lower than the Co-rich alloys. It is well-known that the frequency dependence of the excess loss component per cycle follows a power law close to $f^{1/2}$ [20]. However, specific anomalies can deviate the power-law dependence at high frequencies [20]. The difference in the slopes of the investigated alloys can be explained as a change in the balance between magnetization rotation and domain wall motion, frequency-dependent skin

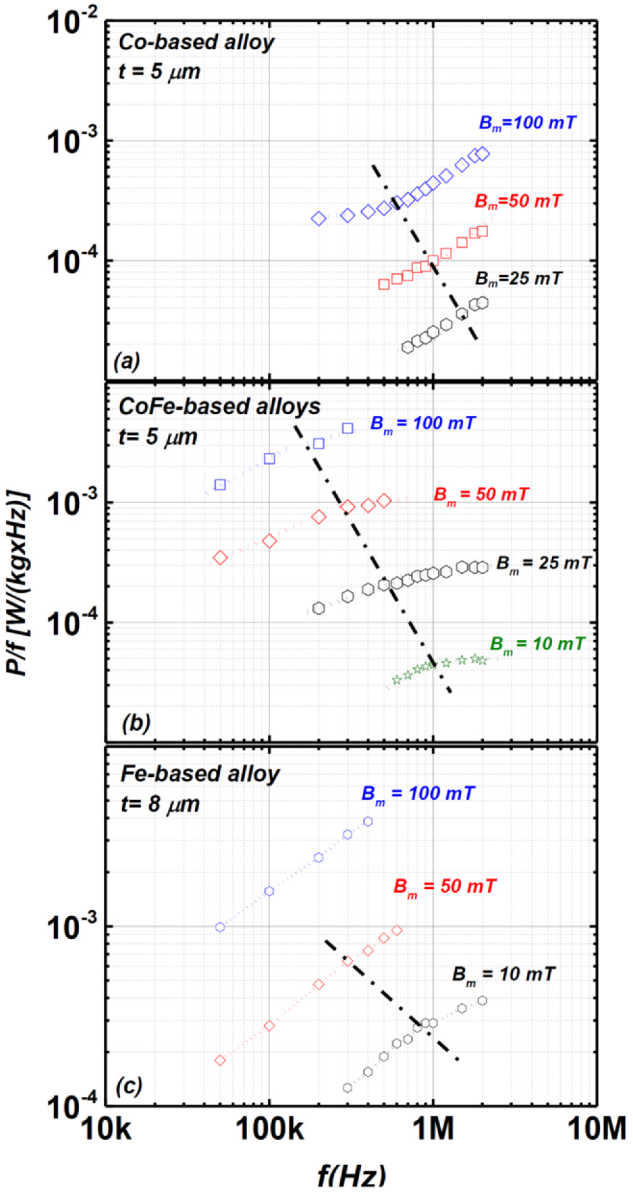

Fig. 4. Core loss per cycle (P/f) versus f of 5 μm as-quenched amorphous ribbons of (a) Co-rich alloy, (b) CoFe-rich alloy, and 8 μm as-quenched amorphous ribbon of (c) Fe-rich alloy at different excitation fields (B_m). The dash-dotted line is used as a guide to show the eddy-excess transition frequency for the investigated alloys.

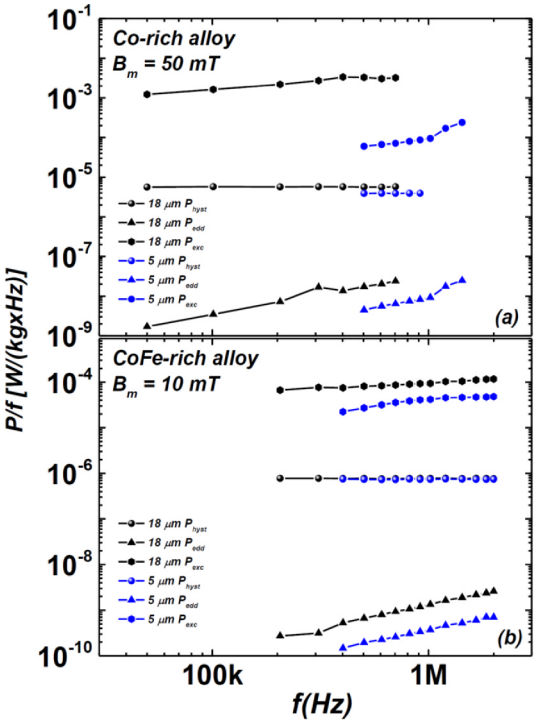

Fig. 5. Material loss decomposition of total loss (P) into Hysteresis loss (P_{hys}), Eddy-current loss (P_{edd}), and Excess loss (P_{exc}) for (a) Co-rich alloys, (b) CoFe-rich alloys.

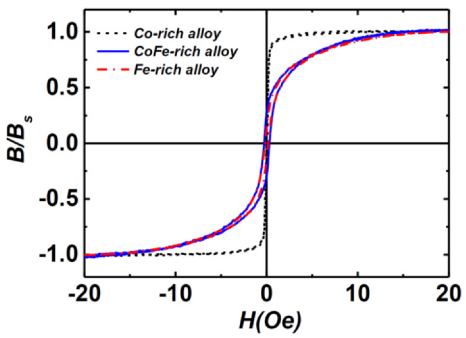

Fig. 6. Major hysteresis loops of as-quenched Co–, CoFe- and Fe-rich amorphous alloys measured using ribbons of length 25 mm at the maximum field of ~ 80 kA/m.

effects, and magnetic resonance phenomenon [20].

In order to understand the material's loss mechanisms, a precise description of the magnetization reversal of each alloy was investigated using hysteresis loops. Fig. 6 presents the typical quasistatic hysteresis loops of the investigated alloys. It is well-known that the balance between the domain wall motion and moment rotation governs the shape and area of the hysteresis loop [24]. The different shape of major hysteresis loops (Fig. 6) suggests that the dominant magnetization reversal mechanisms may vary among the investigated alloys. In addition, a significant difference in the H_c of the Co-rich (~3.2 A/m), CoFe- (~23.9 A/m) and Fe-rich (~15.9 A/m) alloys was measured, which could be attributed to the different levels of residual stress, owning to different magnetostriction constants of alloys, produced during the quenching process of the alloys.

Magnetization reversal modes are crucial in understanding the fundamental mechanisms responsible for material losses at high frequencies. The magnetization reversal modes inside the bulk samples can be determined by the shape of the hysteresis loops and the dependence of the remanence magnetization (B_r), based on minor hysteresis loops on the maximum induction B_{max} [4]. Fig. 7 presents the detailed minor hysteresis loops of the investigated alloys at various magnetization levels. Varga *et al.* [25] extracted the domain wall movement and magnetization rotation using a magnetization reversal process of an ultra-soft magnetic alloy and concluded that the domain wall displacement generates a square-type hysteresis loop similar to the major loop, while domain rotation reveals a flat loop. A similar explanation can be put forward in the present case. The minor flat loops of the Co-rich alloy suggest that the magnetization reversal was dominantly governed by magnetization rotation while the square shape of the minor hysteresis loops of the CoFe-rich and Fe-rich alloys confirms the major magnetization reversal by domain wall displacement. The difference in the magnetization processes of the Co-, CoFe- and Fe-rich amorphous ribbons might be related to differences in local and average anisotropies resulting from different λ_s of the alloys. In order to confirm this hypothesis, the λ_s of the alloys was measured and summarized in Table 2. The λ_s of CoFe- and Fe-rich alloys was found to be two orders

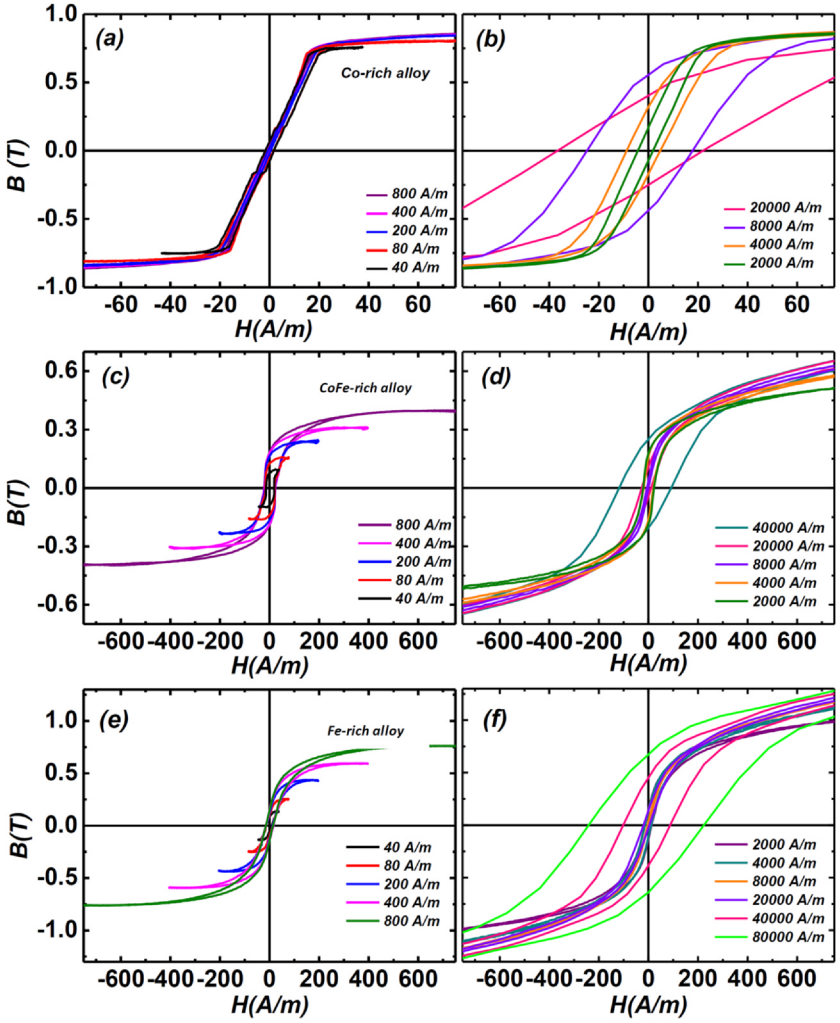

Fig. 7. Minor hysteresis loops of amorphous ribbons of (a), (b) Co-rich alloy, (c), (d) CoFe-rich alloy, (e), (f) Fe-rich alloy.

Table 2
The magnetostriction constant (λ_s) of the as-quenched amorphous Co–, CoFe-, and Fe-rich alloys measured by a small-angle magnetization rotation (SAMR) process.

Sample	λ_s ($\times 10^{-6}$)
Co-rich alloy	0.02
CoFe-rich alloy	1.27
Fe-rich alloy	9.34

of magnitude higher than the Co-rich alloy. In CoFe- and Fe-rich amorphous alloys, the local magnetostrictive anisotropies predominate due to the large λ_s of the alloys, and consequently, extend over larger length scales than the exchange length and, as a result, are not balanced by the exchange interactions [26]. The magnetization reversal process takes place as a domain wall displacement against these local anisotropies. Contrary to the CoFe- and Fe-rich alloys, Co-rich alloys reveal very small magnetostrictive anisotropies due to small $\lambda_s = 0.02 \times 10^{-6}$, and consequently, the magnetization reversal is much easier at low fields, as shown in Fig. 7.

The type of domain walls and nature of domain wall motion in a magnetic field determines the magnetization and magnetization

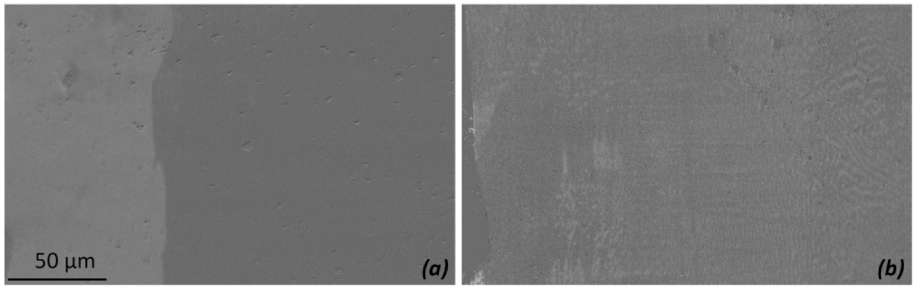

Fig. 8. Magnetic domains imaged by the magneto-optical Kerr effect (MOKE) microscope along the longitudinal ribbon axis of (a) Co-rich amorphous alloy, (b) CoFe-rich amorphous alloy.

reversal in the magnetic materials. However, the observation of magnetic domains in amorphous materials is rather challenging, especially at high frequencies [4]. Another difficulty appears from the absence of magnetocrystalline anisotropy in amorphous materials and, consequently, magnetic domains can only be observed in as-quenched amorphous alloys either with ultra-low residual stress or after inducing uniaxial magnetic anisotropy by post magnetic annealing [4]. Fig. 8 shows the magnetic domains imaged at low frequency using Kerr microscopy, under zero DC magnetic field. Wide and uniform magnetic domains with 180° walls were observed for the Co-rich alloys, while very complex "fingerprint-like" inhomogeneous domains were observed in CoFe-rich alloys. Despite our best efforts, magnetic domains in Fe-rich alloys were not apparent under the same experimental conditions. The orientation of magnetic domains in ferromagnetic systems results from the minimization of magnetic Gibb's free energy, which consists of magnetostatic stray field energy (E_S), anisotropy energy (E_A), and domain wall energy (E_D) [24]. A wide magnetic domain structure appears when the E_S and E_A components are at their lowest levels, and spontaneous magnetization tends to emerge in the in-plane orientation. Contrarily, a complex domain structure, like closure domains, emerges by minimizing the E_S component when the anisotropy axis is perpendicular to the ribbon axis [24]. Residual stress in the amorphous alloys can be a source of strong magnetic anisotropy, especially when λ_s is remarkably high [24]. The high λ_s of CoFe- and Fe-rich amorphous alloys, as compared to Co-rich alloys (see Table 2), makes the alloys highly compressive, and hence leads to the formation of fingerprint-like intricate domain patterns, while the 180° domain walls observed in Co-based alloys are the result of comparatively small residual stress due to zero/near-zero λ_s [24]. The high level of residual stress in Fe-rich alloys, induced due to the highest λ_s among the investigated alloys, might be the reason for orienting magnetic domains into a scale below the instrumental limits.

Direct observation of magnetic domains with the evolution of frequency is quite challenging and mostly observed up to the kHz frequency range in amorphous and nanocrystalline materials [27]. However, most recently, Magni *et al.* [28] imaged the magnetic domains up to the MHz range and found the exciting fact that domain wall displacement was progressively damped and, eventually, halted on approaching the MHz range; and consequently, the only dissipation mechanisms emerge from the rotational process [29]. However, at low frequencies, the magnetization process is a combined effect of magnetization rotation and domain wall displacement [27]. As the dominant mechanism of magnetization reversal in CoFe- and Fe-rich amorphous alloys remained domain wall displacement, as shown by minor hysteresis loops, it seems that the excess loss is the major loss component in the investigated frequency range. Therefore, no remarkable improvement in the material performance was observed even after reducing the thickness of alloys. Contrary to that, the contribution of excess loss in Co-rich alloy is significantly small (Fig. 5), due to the magnetization reversal by rotation, and therefore, the reduction of eddy current loss resulted in significant improvement in materials loss performance by in-situ thinning.

4. Conclusions

The high-frequency performance and underlying loss mechanisms in rapidly quenched ultra-thin amorphous ribbons of Co-rich, CoFe-rich, and Fe-rich alloys were investigated to understand the potential of high-flux density soft magnetic amorphous alloys for device miniaturization. The ultra-high performance of Co-rich amorphous alloys at high frequencies, as compared to the CoFe- and Fe-rich alloys, was attributed to the significant reduction in eddy current loss, due to the reduced thickness, and minimum excess loss, due to dominant magnetization rotation reversal mechanism. Contrarily, a marginal improvement in the total loss of the Fe-rich alloys on in-situ thinning was attributed to the excessive contribution of excess loss, due to the large magnetoelastic contributions to complex fingerprint like magnetic domains displacement magnetisation reversal process. The advantage of ultra-thin Co-rich amorphous alloys over the CoFe- and Fe-rich alloys was discussed in relation to their magnetization reversal through the domain rotation process using minor hysteresis loops.

CRediT authorship contribution statement

Ansar Masood: Conceptualization, Data curation, Formal analysis, Investigation, Methodology, Validation, Visualization, Writing - review & editing, Writing - original draft. **H.A. Baghbaderani:** Data curation, Formal analysis, Methodology, Validation, Visualization, Writing - review & editing. **K.L. Alvarez:** Data curation, Formal analysis, Investigation, Methodology, Validation, Visualization, Writing - review & editing. **J.M. Blanco:** Data curation, Formal analysis, Investigation, Methodology, Resources, Validation. **Z. Pavlovic:** Data curation, Formal analysis, Investigation, Methodology, Validation, Visualization. **V. Ström:** Methodology, Resources, Supervision. **P. Stamenov:** Funding acquisition, Project administration, Resources. **C.O. Mathuna:** Funding acquisition, Project administration, Resources. **P. McCloskey:** Funding acquisition, Project administration, Resources, Validation, Writing - review & editing.

Declaration of Competing Interest

The authors declare that they have no known competing financial interests or personal relationships that could have appeared to influence the work reported in this paper.

Acknowledgements

The authors would like to thank the Science Foundation Ireland (SFI) for the financial support to perform the research work under the grant number of 2015/SIRG/3569, Starting Investigator Research Grant (SIRG).

Appendix A. Supplementary data

Supplementary data to this article can be found online at https://doi.org/10.1016/j.jmmm.2020.167469.

References

[1] Glaser, J.S. and J.M. Rivas. A 500 W push-pull dc-dc power converter with a 30 MHz switching frequency. in 2010 Twenty-Fifth Annual IEEE Applied Power Electronics Conference and Exposition (APEC). 2010.
[2] Perreault, D.J., et al. Opportunities and Challenges in Very High Frequency Power Conversion. in 2009 Twenty-Fourth Annual IEEE Applied Power Electronics Conference and Exposition. 2009.
[3] W.C. Li, et al., Magnetic behavior of soft magnetic composites constructed by rapidly quenched flake-like FeSiAl alloy, J. Alloy. Compd. 819 (2020).
[4] N.A. Skulkina, et al., Magnetization processes in ribbons of soft magnetic amorphous alloys, Phys. Met. Metall. 119 (2) (2018) 127–133.
[5] Baghhaderani, H.A., et al., Fabrication and development of miniaturized efficient power converters using ultra-soft magnetic ribbons. 2018 Ieee International Magnetic Conference (Intermag), 2018.
[6] A. Masood, et al., Fabrication and soft magnetic properties of rapidly quenched Co-Fe-B-Si-Nb ultra-thin amorphous ribbons, J. Magn. Magn. Mater. 483 (2019) 54–58.
[7] A. Masood, et al., Effect of Ni-substitution on glass forming ability, mechanical, and magnetic properties of FeBNbY bulk metallic glasses, J. Appl. Phys. 113 (1) (2013).
[8] K. Ackland, et al., Ultra-soft magnetic Co-Fe-B-Si-Nb amorphous alloys for high frequency power applications, AIP Adv. 8 (5) (2018).
[9] E. Dastanpour, et al., On the glass forming ability (GFA), crystallization behavior and soft magnetic properties of nanomet-substituted alloys, J. Non-Cryst. Solids 529 (2020).
[10] S. Kulkarni, et al., Low loss magnetic thin films for off-line power conversion, IEEE Trans. Magn. 50 (4) (2014).
[11] Lee, S., et al., Magneto-Thermo-Gravimetric technique to investigate the structural and magnetic properties of Fe-B-Nb-Y Bulk Metallic Glass. 13th International Conference on Rapidly Quenched and Metastable Materials, 2009. 144.
[12] K. Narita, J. Yamasaki, H. Fukunaga, Measurement of saturation magnetostriction of a thin amorphous ribbon by means of small-angle magnetization rotation, IEEE

Trans. Magn. 16 (2) (1980) 435–439.
[13] K.L. Alvarez, et al., Novel Fe-based amorphous and nanocrystalline powder cores for high-frequency power conversion, J. Magn. Magn. Mater. 501 (2020) 166457.
[14] K.L. Alvarez, et al., Structural and magnetic properties of amorphous and nanocrystalline Fe-Si-B-P-Nb-Cu alloys produced by gas atomization, J. Alloy. Compd. 810 (2019).
[15] T. Bitoh, A. Makino, A. Inoue, Origin of low coercivity of Fe-(Al, Ga)-(P, C, B, Si, Ge) bulk glassy alloys, Mater. Trans. 44 (10) (2003) 2020–2024.
[16] R. Piccin, et al., Magnetic properties and power losses in Fe-Co-based bulk metallic glasses, J. Magn. Magn. Mater. 320 (20) (2008) E806–E809.
[17] G. Bertotti, Hysteresis in magnetism, Academic Press Limited, United State of America, 2008.
[18] E. Barbisio, F. Fiorillo, C. Ragusa, Predicting loss in magnetic steels under arbitrary induction waveform and with minor hysteresis loops, IEEE Trans. Magn. 40 (4) (2004) 1810–1819.
[19] G. Bertotti, et al., Hysteresis in magnetic materials: the role of structural disorder, thermal relaxation, and dynamic effects, J. Magn. Magn. Mater. 226 (2001) 1206–1212.
[20] C. Appino, et al., Magnetization process and magnetic losses in field-annealed amorphous and nanocrystalline ribbons, J. Optoelectron. Adv. Mater. 6 (2) (2004) 511–521.
[21] Roshen, W.A., Thin amorphous films for power magnetic components. Apec 2007: Twenty-Second Annual Ieee Applied Power Electronics Conference and Exposition, Vols 1 and 2, 2007: p. 63-70.
[22] T. Suzuki, P. Sharma, A. Makino, Extending the operational frequency range of high B – FeSiBP amorphous alloy to GHz by coating the powder surface with silicon oxide, J. Magn. Magn. Mater. 491 (2019) 165641.
[23] T. Suzuki, P. Sharma, A. Makino, Extending the operational frequency range of high B-s - FeSiBP amorphous alloy to GHz by coating the powder surface with silicon oxide, J. Magn. Magn. Mater. 491 (2019).
[24] S. Mallick, et al., Static and dynamic behavior of domain walls in high B-S soft magnetic ribbons tuned by the annealing temperature, J. Phys. D-Appl. Phys. 51 (6) (2018).
[25] L.K. Varga, G. Kovacs, Separation of magnetization loop in domain wall movement and domain rotation contributions for soft magnetic materials, Acta Phys. Pol. A 113 (1) (2008) 159–162.
[26] J. Kovac, L. Novak, L.K. Varga, Study of the magnetization processes in amorphous and nanocrystalline FINEMET by the numerical decomposition of the hysteresis loops, Acta Phys. Pol. A 131 (4) (2017) 732–734.
[27] S. Flohrer, et al., Dynamic magnetization process of nanocrystalline tape wound cores with transverse field-induced anisotropy, Acta Mater. 54 (18) (2006) 4693–4698.
[28] A. Magni, et al., Fluxmetric-magnetooptical approach to broadband energy losses in amorphous ribbons, J. Appl. Phys. 109 (7) (2011).
[29] A. Magni, et al., Magnetization process in thin laminations up to 1 GHz, IEEE Trans. Magn. 48 (4) (2012) 1363–1366.